Testing ground based observations of wave activity in the (lower and upper) atmosphere as possible (complementary) indicators of streamer events

Michal Kozubek[1], Lisa Kuchelbacher[2], Jaroslav Chum[1], Tereza Sindelarova[1], Franziska Trinkl[2, a], Katerina Podolska[1]

[1]Institute of Atmospheric Physics CAS, Bocni II 1401, Prague, 14100, Czech Republic

[2] Earth Observation Center, Deutsches Zentrum für Luft- und Raumfahrt,82234 Weßling, Germany

[a] now at Karlsruhe Institute of Technology (KIT), Institute of Meteorology and Climate Research, Karlsruhe, Germany

Correspondence: Michal Kozubek, kom@ufa.cas.cz

Keywords: gravity waves, streamer events, infrasound, Doppler measurements

Abstract: For a better understanding of atmospheric dynamics, it is very important to know the general condition (dynamics and chemistry) of the atmosphere. Planetary waves (PWs) are global scale waves, which are well-known as main drivers of the large-scale weather patterns in mid-latitudes on time scales from several days up to weeks in the troposphere. When PWs break, they often cut pressure cells off the jet stream. A specific example are so-called streamer events, which occur predominantly in the lower stratosphere at mid- and high-latitudes. For streamer events we check, whether there are any changes of gravity wave (GW) or infrasound characteristics related to these events in ionospheric and surface measurements (continuous Doppler soundings, two arrays of microbarometers) in the Czech Republic.

Phenomena in infrasound arrival parameters undoubtedly related with streamer events were not identified in observations of two stations located in Central Europe. Simulations of infrasound propagation show influences of the streamer events on the waveguide formed near the tropopause. Microbarom propagation is influenced by the tropopause waveguide in a limited azimuth sector and at limited distances. Due to the typical occurrence of the streamer events over the North Atlantic, infrasound stations in Western Europe can be of particular interest for future studies of streamer event signatures in infrasound arrivals. Arrivals to Central Europe are through the waveguide formed between the ground and the upper stratosphere. The upper stratosphere waveguide is not influenced by the streamer events.

Supplementary ground-based measurements of GW using the WBCI array in the troposphere showed that GW propagation azimuths were more random during streamer and streamer-like events compared to those observed during calm conditions. GW propagation characteristics observed in the ionosphere by continuous Doppler soundings during streamer events did not differ from those expected for the given time period.

1) Introduction

For a better comprehension of climate change it is fundamentally important, how well we understand the climate system in general, and the dynamics of the atmosphere in particular. The dynamical processes relevant in this context in the atmosphere take place over a comparatively wide range of scales in space and time. They include in particular both, planetary and gravity waves. Planetary waves are the main drivers of the extratropical circulation. When they break, they lead to an irreversible exchange of air masses between the equatorial and polar region due to an amplification of their amplitudes (e.g. McIntyre & Palmer, 1983; Polvani & Plumb,1992). In the lower stratosphere ozone can be used as a tracer for these large-scale motions, as it has a comparatively long life-time. When planetary waves break tropical air masses of low ozone concentration are mixed poleward into the sourrounding atmosphere of the mid and higher latitudes (e.g. Leovy et al., 1985).

The term "streamer" lacks a precise definition, as noted by Krüger et al. (2005). They discuss various aspects of streamers, including their impact on mixing and the divergent definitions associated with them. Offermann et al. (1999) describe streamers as large-scale tongue-like structures formed by the meridional deflection of air masses. Streamers are characterized by irreversible mixing of air masses between equatorial and polar regions which is why they might be linked to planetary wave breaking (Waugh, 1993). Eyring et al. (2003) give a climatology of the seasonal and geographical distribution of streamer events. They show, that streamers often occur over the Northern Atlantic and can be identified by either high NO_2 or low ozone concentration, which is why we select streamers by total ozone column measurements. They show that streamer events occur most often during winter and least during July and August in the Northern Hemisphere. During a streamer event the wind field changes rather strong over a comparatively small distance. Since a streamer event shows a strong wind shear at its flanks, it is expected that it excites GW (e.g. Kramer et al., 2015 and 2016 or Peters et al., 2003).

It is well-known that enhanced wind gradients or anticyclones can lead to the excitation of gravity waves (GW) in the atmosphere (e.g. Pramitha et al., 2015; Kai et al., 2010; Kramer et al., 2015, 2016 and Gerlach et al., 2003). GW have typical vertical wavelengths from a few 100 m to several kilometres (Wüst & Bittner, 2006), and horizontal wavelenghts over tens of km (Wüst et al., 2018), and longer (Rauthe et al., 2006); their fluctuations in the upper troposphere / lower stratosphere typically show amplitudes of 5–10 m/s at maximum (e.g., Kramer et al., 2015). Those waves transport energy and momentum horizontally and vertically through the atmosphere and deposit them especially in the stratosphere and mesosphere but also above and below this height region. The propagation of GWs is strongly dependent on the wind conditions in the stratosphere since the wind speed of the middle atmosphere (10–100 km) reaches its maximum there. That is why monitoring waves in upper parts of the atmosphere, e.g. based on Doppler observations in the ionosphere, can provide additional information about stratospheric conditions (for details see Fritts and Alexander, 2003).

Using pressure recordings at a microbarograph array, GWs and infrasound at the ground can be observed. Ground based observations of GWs at a large aperture microbarograph array are utilized in the present study as an independent data source for the analysis of GW activity during streamer events. Infrasound propagation is influenced by wind and temperature fields in the atmosphere. Three regions play an important role in long-distance infrasound propagation: (1) the lower thermosphere; (2) the stratosphere; (3) the jet stream near the tropopause and inversion layers in the troposphere (Evers and Haak, 2010). Infrasound observed at the ground and emitted by distant sources mostly propagates in the stratospheric waveguide (Ceranna et al., 2019). The thermospheric waveguide is not as efficient as the stratospheric waveguide in the long-range infrasound propagation. Besides signal loss due to geometrical spreading, infrasound absorption is important in the upper atmosphere (Bittner et al., 2010). Infrasound absorption is proportional to the frequency; higher frequencies, particularly those above 1 Hz undergo stronger absorption in the thermosphere (Sutherland and Bass, 2004). Signal attenuation is low at frequencies of the order of $10^{-3} – 10^{-2}$ Hz (Blanc, 1985; Georges, 1968).

A number of case studies have proved that stratospheric dynamics can be deduced from microbarograph measurements at the ground (Assink et al., 2014; Blixt et al., 2019; Evers and Siegmund, 2009; Evers et al., 2012; Garcès et al., 2004; Le Pichon and Blanc, 2005; Le Pichon et al., 2006 and 2009; Smets and Evers, 2014). Streamer events are significant transient disturbances to circulation patterns in the tropopause/lower stratosphere region; modifications of the stratospheric waveguide can therefore be expected. A feasibility study on utilisation of ground infrasound measurements in research of streamer events is performed. Its aim is to identify phenomena in infrasound detections related to the streamers; we focus on deviations of the azimuth of signal arrivals, trace velocity, signal amplitude, and frequency. The dedicated studies demonstrated that from the observed signal trace velocity, information about the signal refraction height can be derived (Lonzaga, 2015). If the source of received signals is well defined in time and space, mean atmospheric cross-winds along the signal propagation path can be estimated from back-azimuth deviations and time of signal propagation (Blixt et al., 2019). Fluctuations of signal frequency and amplitude are, besides variability of the signal source influenced by atmospheric filtering (Sutherland and Bass, 2004).

Our study will focus on possible utilization Doppler sounding and microbarographs for description and analysis of GW behaviour and propagation in the stratosphere.

The structure of the paper is as follows: After introduction the description of the used dataset and method can be found in the second section. Then we describe our results and in the last section we discuss the possible connection to previous studies.

2) Data and methods

The selection of streamer events is based on the visual inspection of global maps of total ozone column (TO3), accessible through a service provided by DLR (https://atmos.eoc.dlr.de/) measured by the Tropospheric Monitoring Instrument (TROPOMI) aboard the Sentinel 5 Precursor (S5P) mission. See Veefkind et al., 2012 for details about TROPOMI/S5P. In cases where TROPOMI/S5P data is unavailable, measurements from the Global Ozone Monitoring Experiment-2 (GOME-2) on the Metop series of satellites are utilized. Both instruments operate in a nadir-viewing configuration on near-polar sun-synchronous orbits. Further specifics regarding TO3 measurements by TROPOMI/S5P are elaborated by Spurr et al. (2022). The TO3 retrieval process is built upon the predecessor instrument's processor, with GOME-2 on Metop-AB, see Munro et al. (2006) and Munro et al.

(2016). For detailed information on the GOME-2 retrieval algorithm, refer to Loyola et al. (2011).

We define a streamer as such when the ozone column concentration of the finger-like structure above the Northern Atlantic/Western Europe is lower than 300 DU and persists for at least 3 days. The longitudinal extension is of approx. 15 to 30 degrees in the mid-latitudes (between 30 to 70°N). The northernmost point of a streamer exceeds 50°N. Fig. 1 shows a streamer event above the Northern Atlantic, indicated by the blue color which represent the low ozone concentrations. The streamer shown in Ffig. 1 reaches latitudes beyond 70°N, which indicates a large example. At the western and eastern flanks of the streamer, the ozone concentration exceeds 350 DU, defining distinct boundaries. This is also visible in fFig. 1 represented by the green colors at the eastern coast of Northern America and western Europe. So, there is a gradient of the ozone concentration of about 50 DU / 5°. Furthermore, the streamer exhibits a discernible pattern of circulation, with air masses being meridionally deflected, contributing to its formation and maintenance. These air masses, characterized by their movement from south to north at the eastern flank and from north to south at the western flank, play a significant role in the streamer's dynamics. This is the reason why equatorial low ozone concentration is transported northward. In contrast, the calm periods, representing the opposite dynamic situation to the streamer events, are characterized by only very few meridionally deflected air masses. During these periods, the ozone concentration in the mid-latitudes above the Northern Atlantic is consistently higher than 350 DU, indicating stable atmospheric conditions and minimal perturbations in the ozone distribution. An example for a calm period is shown in Fig. 2.

The streamer events are selected by eye for this study (results see Table 1) considering the TO3 global maps from January 2020 and March 2021. As planetary waves are permanently disturbing the atmospheric dynamic of the higher troposphere / lower stratosphere, especially smaller scale streamers can be observed almost every day and the identification of streamer events becomes subjective. We therefore focus on few events which are comparatively strong in their evolution from our perspective. Moreover, we focus on streamer events above the Northern Atlantic. Whenever another streamer event occurs somewhere other than over the Northern Atlantic region with comparable spatiotemporal extent, we do not consider this date as a streamer event. We assume that the effects of the streamer superimpose and a distinct backtrack to the streamer over the Northern Atlantic will not be possible. This means, that the analysis of the streamer events can be blurred to some extent.

We consider dates from January 2020 to April 2021. In general, planetary waves drive the Brewer Dobson Circulation in the stratosphere during winter and ozone-poor airmasses are transported northward. Streamer events are therefore detected between September and March. The streamer events are distinguished if they have a large spatial size, high intensity (low TO3 concentration) and if air masses are irreversibly mixed into the surrounding atmosphere. All the selected events persist for several days, but no longer than 10 days.

To evaluate whether streamer events effect the smaller-scale atmospheric dynamics, calm events are identified as well by subjective criteria. These events serve as a reference to streamer events, as large-scale spatial structures are hardly visible in the TO3. The events are selected when the ozone concentration shows a meridional gradient from the equator to polar region on the Northern Hemisphere with almost no longitudinal variation. The examples of calm atmospheric dynamics are listed in Table 1 (right).

Streamer events		**Calm periods**	
From	**To**	**From**	**To**
06.02.2020	10.02.2020	02.03.2020	08.03.2020
11.2.2020	13.2.2020	09.03.2020	14.03.2020
31.08.2020	03.09.2020	28.03.2020	10.04.2020
05.09.2020	11.09.2020	19.04.2020	27.05.2020
03.11.2020	07.11.2020	9.11.2020	15.11.2020
21.11.2020	25.11.2020	12.12.2020	22.12.2020
23.02.2021	27.02.2021	30.12.2020	06.01.2021
09.03.2021	12.03.2021	21.01.2021	20.02.2021
		28.02.2021	07.03.2021
		13.03.2021	24.03.2021
		29.03.2021	07.04.2021

Table 1 Streamer events above Northern Atlantic from January 2020 until March 2021 and related start and end dates. The right part shows calm periods.

Figure 1 shows the TO3 by TOPOMI/S5P integrated from November 3rd to November 5th 2020. Ozone-poor airmasses (blue) are located above the Northern Atlantic from 30°N to 70°N next to smaller scale ozone-poor airmasses above western North America and Central Asia. The TO3 concentration is disturbed by planetary waves along the latitudes, which lead to wave structures visible especially at the transition of blue to green colors. A large streamer event of ozone-poor airmasses is detected over the Northern Atlantic. A small streamer can be detected over western North America. There are also ozone-poor air masses above eastern Europe. The temporal evolution shows, that the ozone-poor air masses above eastern Europe are due to a decaying streamer which evolved several days earlier. As planetary waves are more or less permanently disturbing the atmospheric dynamics, especially smaller scale streamers can be detected almost every day. In this example, the streamer event above the Northern Atlantic is largest. Therefore, we consider this event for the further analysis.

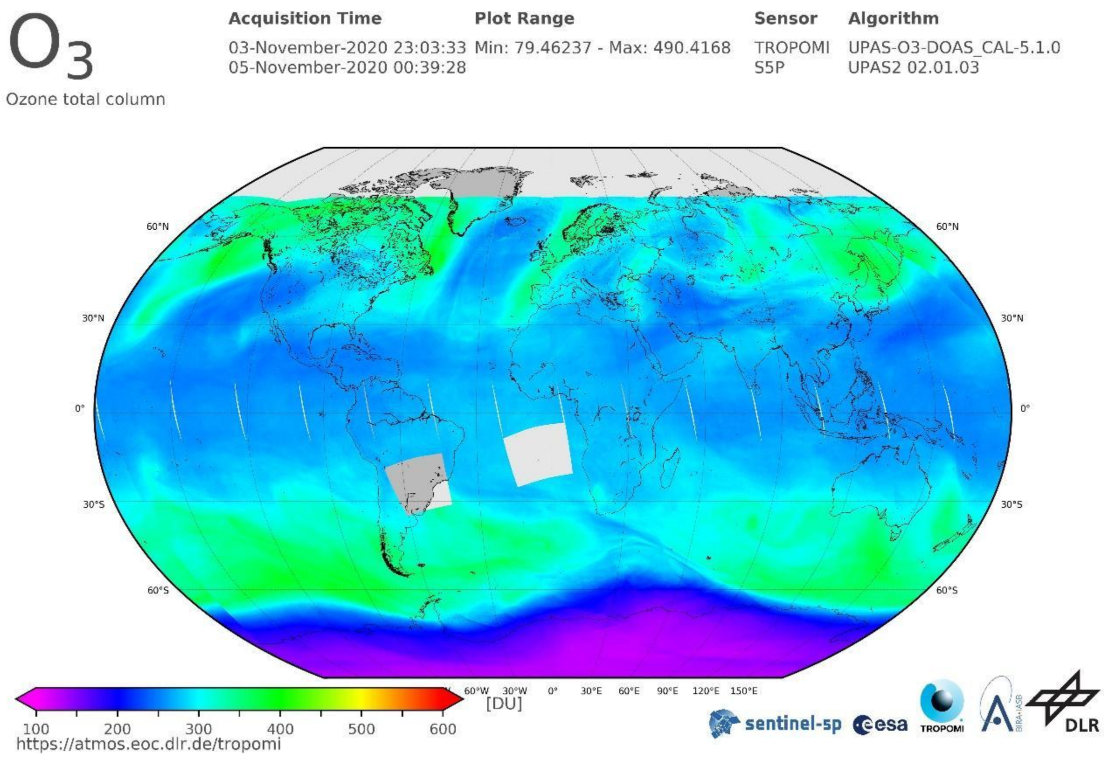

Fig. 1. TO3 by TROPOMI/S5P from November 3^{rd} to November 5^{th} 2020 shows ozone poor airmasses above the Northern Atlantic as an example of a streamer event for the further analysis. Colors (from violet to red) indicate the total ozone column concentrations (from low to high) in Dobson Units. Source: DLR, CC-BY 3.0

Figure 2 shows the TO3 by TOPOMI/S5P from February 11^{th} to February 13^{th} 2020. The event is characterized by a strong meridional gradient from the equatorial to polar region on the Northern Hemisphere with almost no longitudinal variation. Therefore, we consider this event for the further analysis.

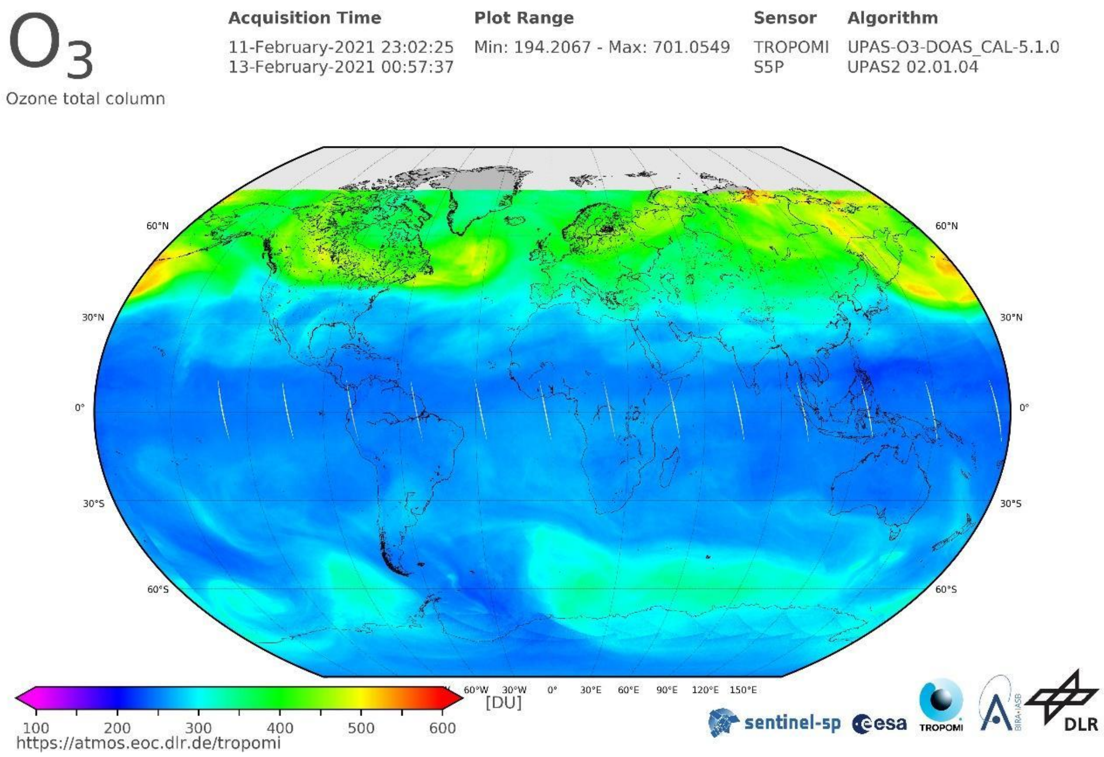

Fig. 2. TO3 by TROPOMI/S5P from February 11^{th} to February 13^{th} 2020 as an example of calm atmospheric dynamics. A clear meridional gradient of ozone can be observed on the Northern Hemisphere without large-scale wave structures. Colors (from violet to red) indicate the total ozone column concentrations (from low to high) in Dobson Units. Source: DLR, CC-BY 3.0

Two stations of the Czech microbarograph network (Bondar et al., 2022) are involved in the study – the large aperture array WBCI (50.25°N 12.44°E) and the small aperture array PVCI (50.52°N 14.57°E). To study propagation of GW and long-period infrasound (from acoustic cut-off up to about 2.5 s) pressure recordings at WBCI are utilized. Four sensors of the WBCI array are arranged in a tetragon. The inter-element distances of 4 – 10 km define an optimum performance of the array in the infrasound frequency range from the acoustic cut-off frequency of 0.0033 to 0.0068 Hz (Garcès, 2013). The WBCI array with its large inter-element distances has a unique configuration compared to the arrays of the International Monitoring System of the Comperehensive Nuclear Test Ban Treaty Organisation intended for infrasound monitoring in the frequency band of 0.02 – 4 Hz (Marty, 2019). Each array element at WBCI is equipped with an absolute microbarometer of the type Paroscientific 6000-16B-IS with parts-per-billion resolution. A GPS receiver is used for time stamping. Data are stored with a sampling rate of 50 Hz. For infrasound monitoring, WBCI data are resampled at 10 Hz sampling rate. To detect and analyze GW, 1-min mean values of the absolute pressure data are used.

The small aperture array PVCI provides optimal precision of detections in the frequency range of 0.14 – 3.4 Hz (Garcès, 2013). Three sensors are arranged in an equilateral triangle; the array aperture is 200 m. The differential sensors of the type Infrasound Gage ISGM03 manufactured by the Scientific and Technical Centre give a flat response in the frequency range of 0.02 – 4 Hz. A GPS receiver is used for time stamping. The data are stored with a sampling frequency of 25 Hz. This sampling rate is also used in regular processing of infrasound detections at PVCI.

Infrasound detections are processed using the DTK-GPMCC software the core of which is the Progressive Multi-Channel Correlation (PMCC) detection algorithm (Cansi, 1995; Le Pichon and Cansi, 2003). PMCC analyses pressure recordings from an infrasound array and looks for coherent signals in overlapping time windows in several frequency bands (Le Pichon and Cansi, 2003). An elementary detection with the PMCC, or the detection pixel is declared in the time-frequency window, when signal correlation and consistency criteria are met. Detection pixels are grouped into the detection families based on similar time, frequency, azimuth of signal arrival, and signal trace velocity (Brachet et al., 2010). The arrival parameters of the detected infrasound are stored in the detection bulletins. The parameters of interest for the present study include time of arrival, azimuth of arrival, trace velocity, frequency, and amplitude. The PMCC configuration is set on an individual basis and is optimized for the given array (Brachet et al., 2010; Garcès, 2013; Szuberla et al., 2004); main parameters of the DTK-GPMCC settings for the arrays PVCI and WBCI are given in Table 2.

Station	PVCI	WBCI
Detection range	0.09-7 Hz	0.0033-0.4 Hz
Number of detection bands	19	11

Length of the detection window; frequency dependent	412.84-6.44 s	2555-118 s
Adjacent windows overlap	95 %	90 %
Consistency	0.1 s	3 s
Azimuth tolerance for families forming	10°	3°
Family size	10-50 pixels	15-50 pixels
Frequency range analysed in the study of streamer events	0.09-0.4 Hz	0.0033-0.4 Hz

Table 2. Main parameters of the DTK-GPMCC configurations for the arrays PVCI and WBCI.

InfraGA/GeoAc raytracing tools are employed to study infrasound ducting in the atmosphere (Blom and Waxler, 2012; Blom, 2019). Infrasound raytracing can reveal possible modifications of atmospheric waveguides above the Eastern Atlantic and Western Europe during streamer events. Streamer events influence the tropopause and lower stratosphere. Hence, modifications of the stratospheric waveguide are expected rather than its entire reversals or collapse. Raytracing can identify azimuths and distances from the source that are influenced by a streamer event. And so, it can reveal whether these influences reach Central Europe or the signals are ducted to the region through the waveguide in the upper stratosphere or thermosphere like in quiet periods. InfraGA/GeoAc provides simulations of signal propagation from a point source; propagation through the range dependent atmosphere is modelled in the present study. Atmospheric characteristics are obtained from the G2S model (Drob et al. 2003). Vertical profiles of temperature, zonal and meridional winds, density and pressure are an input for the InfraGA/GeoAc. The grid of profiles covers the area from 45° to 65°N and from 30°W to 22.5°E; latitudinal step is 5° and longitudinal step is 7.5°.

Propagation of GW in the thermosphere/ionosphere is studied using the multi-point and multi-frequency continuous Doppler sounding system located in Czechia. Its advantage is a high time resolution (around 10 s) compared with ionospheric sounders (ionosondes) that measure the profile of electron densities in the ionosphere. The frequency shift is due to the motion and electron density changes in the ionospheric plasma, caused for example by interaction with atmospheric waves propagating in the neutral atmosphere, with which the ionosphere (above ~ 80 km) merges. The sounding radio signal is reflected at the height, where its frequency matches the so called local plasma frequency, which is determined by the local electron density. Therefore, the reflection height changes during the day and depends on the sounding frequency. Significant Doppler shifts, usable for analysis, are obtained if the signal is reflected from the so called F2 layer (approximately 200 – 300 km). Several sounding frequencies are used in Czechia. The 3.59 MHz sounding was mostly effective at night, while the 4.65 MHz sounding provided good daytime data during the period analyzed. The propagation characteristics of GWs are calculated from the time delays between signals observed at the respective sounding paths (reflection points for each transmitter-receiver pairs) assuming that the reflection points are in the midpoints between each transmitter and receiver. A 60 or 90 min long time interval is usually used to calculate the velocities and azimuth of the observed waves. The methods are in detail described by Chum and Podolska (2018). The two-dimensional (2-D) version (propagation analysis in horizontal plane only) is anticipated for most of the studies, since a 3-D analysis requires simultaneous observation and signal correlation at different frequencies, which is often not the case, especially during solar minimum. Results of statistical investigation have been recently published (Chum et al., 2021). Identical methods of propagation analysis have been applied to investigate propagation of GWs in the troposphere based on data from large-aperture array WBCI (here the time delays are related to the locations of individual microbarometers). All analyses will be done with respect to the streamer events and calm periods shown in Table 1.

3) Results

3.1 Infrasound observations at ground microbarograph arrays WBCI and PVCI in November 2020 and in March 2021

Wave activity in the infrasound frequency range of 0.0033-0.4 Hz is investigated combining observations at the stations WBCI and PVCI. Infrasound detections at WBCI are processed in the frequency band of 0.0033 – 0.4 Hz. The operational range of the array is extended above the upper limit of the optimum array range; the degraded performance of WBCI at frequencies higher than 0.0068 Hz shall be considered. The upper limit of the analysed band is intentionally set to 0.4 Hz to cover microbaroms. PVCI detections are analysed in the frequency range of 0.09 – 0.4 Hz. The band partly overlaps with the detection range of the WBCI array and at frequencies of 0.12 – 0.35 Hz it is dominated by microbaroms (e.g., Campus and Christie, 2010). Unlike WBCI, PVCI provides an optimal performance in the microbarom band.

Microbaroms are infrasound signals generated by a non-linear interaction of ocean waves travelling in opposite directions. Microbaroms form a wide peak around 0.2 Hz in the infrasound spectrum; their frequency corresponds to twice the frequency of sea waves. A powerful source of microbaroms is located in the North Atlantic and the signals are regularly detected by European stations (Hupe et al., 2019). The detection capability of microbaroms from the North Atlantic is particularly high from October to March when the source becomes stronger due to stormy weather above the ocean and signal propagation to the East from the source is supported by the stratospheric waveguide (Landès et al., 2012). From the global point of view, microbaroms are permanently present in recordings of infrasound stations worldwide.

Streamer events often occur above the North Atlantic. Thus, microbaroms propagating from the North Atlantic to the continental Europe can travel through the region influenced by a streamer event and the detections at infrasound stations in Europe can show signatures of streamer events.

We analyse infrasound observations from 3^{rd} to 25^{th} November 2020 and from 28^{th} February to 25^{th} March 2021 with focus on microbaroms. In these time intervals adjacent streamers and calm periods occurred (Table 1). Streamers and the calm period in the November 2020 time window are evaluated separately from those in the March 2021 time window to avoid seasonal influences. While a well-developed eastward stratospheric waveguide can be expected in November, its efficiency can decrease in March due to the seasonal reversal of stratospheric winds.

3.1.1 Infrasound observations from 3^{rd} to 25^{th} November 2020

Two streamer events developed in November 2020. The first streamer occurred from 3^{rd} to 7^{th} November and the second one from 21^{st} to 25^{th} November. The streamers were separated by a calm period from 9^{th} to 15^{th} November.

The most important phenomena found in the infrasound arrival parameters are fluctuating signal frequency and fluctuating signal amplitude.

WBCI provides rather sparse detections during both streamer events and only two detection families are obtained during the seven-day calm period (Figure 3). The ~~signal~~ frequencies near 0.2 Hz and back-azimuths of 290° – 350° indicate that the observed signals are likely microbaroms from the North Atlantic. A decrease of the signal frequency is observed during the first streamer event. On 5th – 6th November from 20 to 05 UTC, the mean frequency of the north-west arrivals drops down to 0.04 Hz, below the microbarom frequency range. During the second streamer event from 21st to 25th November, the signal frequency is stable around 0.22 Hz. An increase of the amplitude from the mean value of 0.019 Pa to 0.035 Pa is observed from 23rd November, 18 UTC until the end of the analysed time period on 25th November at 24 UTC.

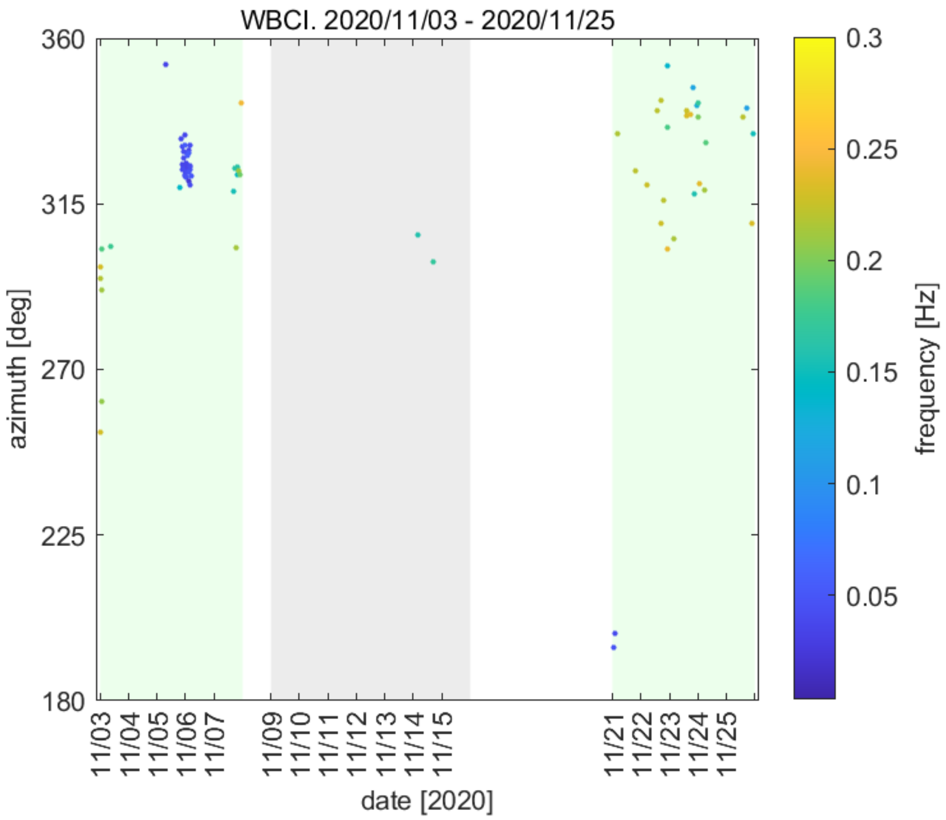

Fig. 3. Infrasound observations at WBCI on 3rd - 25th November 2020. Azimuth of signal arrivals is shown; the colorbar refers to the mean frequency of the detection family. One circle in the plot represents one detection family. Green background marks the streamer events, grey background marks the calm period.

Similar to the back-azimuths at WBCI, PVCI detects arrivals from the north-west in the analysed frequency range of 0.09 – 0.4 Hz (Figure 4). Fluctuating signal amplitudes are observed. Values around 0.020 Pa occur on 3rd November. From 4th November, 18 UTC to 7th November, 22:30 UTC, the signals are of amplitudes around 0.089 Pa. The amplitudes decrease to the values around 0.046 Pa during the following quiet period on 9th – 15th November. Microbarom amplitudes fluctuate between 0.013 and 0.036 Pa (1st decile and 9th decile, respectively) during the streamer event on 21st – 25th November. Publicly available data – meteorological charts provided by Deutscher Wetterdienst and the WAVEWATCHIII® wave-action model (The WAVEWATCHIII® Development Group, 2016) indicate that there are maritime storms in the North Atlantic within the analysed time window from 3rd to 25th November 2020. The storms can cause fluctuating intensity of the microbarom source and as a consequence, fluctuating microbarom amplitudes are observed at the infrasound stations.

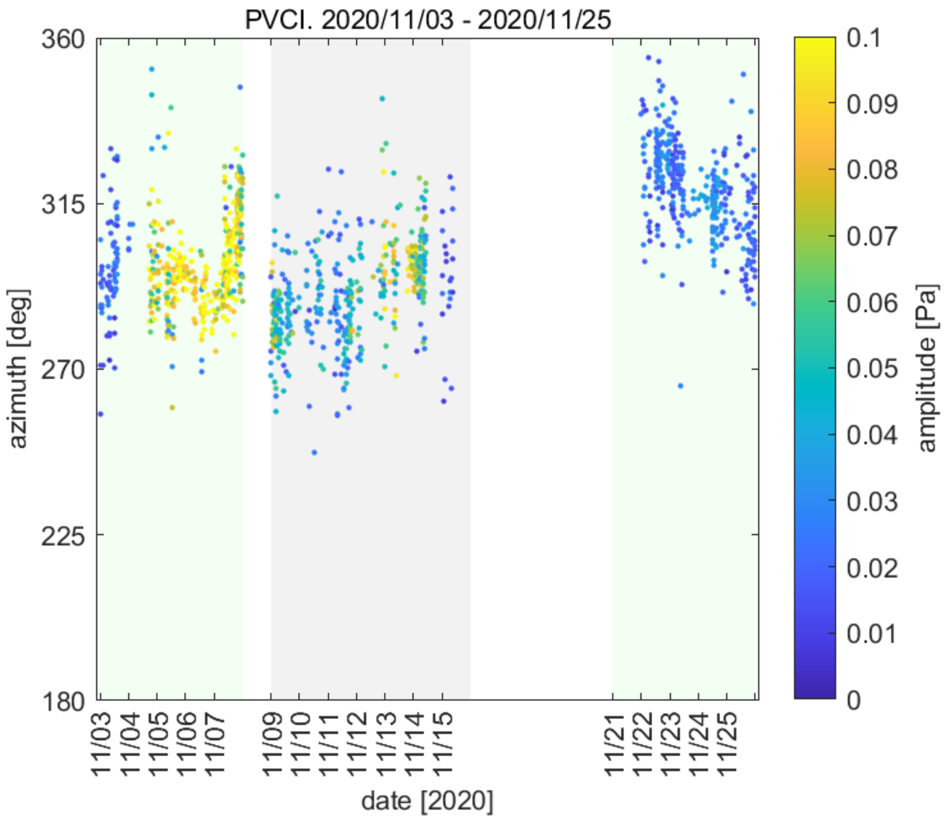

Fig.4. Infrasound observations at PVCI on 3rd - 25th November 2020. Azimuth of signal arrival is shown; the colorbar refers to the signal amplitude. Green background marks the streamer events, grey background marks the calm period.

To study propagation of signals from sources located at the surface of the North Atlantic the InfraGA/GeoAc tools are employed. The fictitious point sources are located (1) at 55°N and 15°W, (2) at 55°N and 5°W, and (3) at 60°N and 0°longitude. The coordinates of the sources are estimated based on the position of the tropopause jet stream disturbance. Point

(1) is located under the northward jet-stream, point (3) under the southward jet-stream, and point (2) is located between those two opposing branches of the jet stream disturbance see Figure 5.

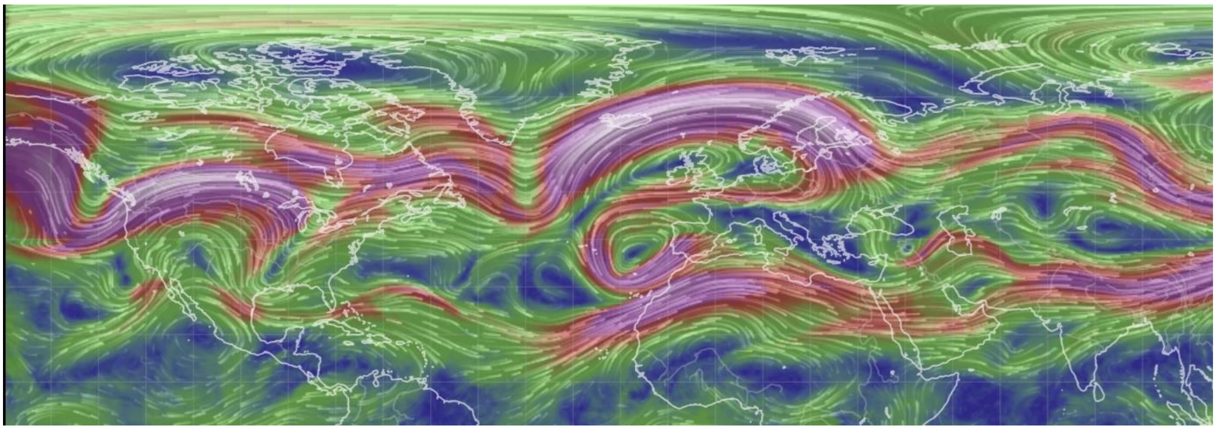

Fig.5. Wind field at the pressure level of *250 hPa* on 06 November 2020 at 00 UTC. A disturbance of the jet-stream above the eastern North Atlantic and the British Isles is caused by the streamer event.

A multi azimuth simulation is run on 6th November at 00 UTC, during the streamer event. Taking into account the mutual locations of the sources and the receiving arrays, eastward signal propagation is modelled. The azimuth limits are set to 0° and 180°, the azimuth step is 3°. Signal inclinations 2° – 45° are considered in 2° resolution. Information is obtained through which waveguides the signal can possibly arrive to the infrasound stations and their surroundings. The reason why arrivals to the larger areas are considered is that signal propagation from three fictious point sources stands in for an areal source, the surface of the North Atlantic where microbaroms are generated. Therefore, the model outputs must be taken as an approximation of the real situation. The turning height and ground reflections of the 0.2 Hz signal are obtained in the multi azimuth simulation. The results are visualised in Figure 6 and in supplementary materials. The red asterisk represents the point source. The concentric sectors of circles show regions of ensonification, regions where the signal emitted by the source can be recorded at an infrasound station. The dots, signal ground reflections are organized in a radial pattern. Each of the lines of this pattern represents one azimuth of signal propagation for which the multi azimuth simulation is run; the azimuth step is 3°. The colours of the dots inform about the turning height of the ray and thus provide information about signal ducting in the waveguides. Depending on the turning height, infrasound is subject to attenuation of variable strength when it propagates through the atmosphere. Infrasound attenuation is low in the stratospheric waveguide. Strong absorption occurs in the thermospheric waveguide; the absorption is higher at higher signal frequencies (Sutherland and Bass, 2004). To obtain the view of signal attenuation along the raypath in the vertical plain a single azimuth simulation is employed. The single azimuth simulation is run along the azimuths from the fictitious sources (1) – (3) to the stations WBCI and PVCI; it is obtained for the frequencies of 0.04 Hz and 0.2 Hz. As a reference, a multi azimuth propagation of the 0.2 Hz signal is modelled from a source at 55°N and 15°W on the calm day 12th November at 00 UTC.

First, we focus on infrasound propagation from the North Atlantic to Central Europe. Stratospheric and thermospheric ducting are possible from the sources at 55°N 15°W and 55°N 5°W to Central Europe during the streamer event as well as on the calm day (supplementary materials). Signal propagation only through the thermospheric waveguide is enabled from the source at 60°N and 0°longitude (Figure 6). The distances between the fictitious sources and the stations are 1300 – 2000 km. The amplitude loss of the 0.2 Hz signal in the thermospheric waveguide at these distances is 100 dB relative to the amplitude at a distance of 1 km from the source. According to the simulations, observations of the thermospheric arrivals of microbaroms are unlikely at PVCI and WBCI due to strong signal attenuation. Microbaroms apparently arrive to Central Europe through the waveguide formed in the upper stratosphere during the streamer events as well as on the calm day. Indeed, arrivals from the back-azimuths of 285° - 315° are dominant at PVCI o 3rd to 7th November. Those back-azimuths correspond to the sources at 55°N 15°W and at 55°N 5°W, while the back-azimuth to the source at 60°N and 0°latitude is 325°. The amplitude loss of the 0.04 Hz signal at the distances of 1300 – 2000 km from the source is 60 – 80 dB. In general, thermospheric arrivals of this low frequency signal are not strictly rejected. However, in our case the 0.04 Hz signal arrives with trace velocity around 0.330 km/s at WBCI. The low trace velocity indicates signal ducting in the troposphere/lower stratosphere waveguide (Lonzaga, 2015).

Next, we study the influences of the streamer event related disturbance anywhere in the modelled region. The disturbance of the jet stream can modify signal propagation up to distances of several hundreds to a thousand km from the source; the influenced azimuth range is limited. Signals from the source at 55°N and 15°W can propagate in the tropopause waveguide in azimuths between 10° and 60° up to the distance of ~1000 km. The amplitude loss of the 0.2 Hz signal at a distance of 1000 km is 60-70 dB relative to the amplitude at 1 km from the source. The southward branch of the jet-stream disturbance enables infrasound propagation in the tropospheric waveguide in azimuths of 100 - 160° from the source at 60°N 0°longitude. Maximum distance which the signal can travel in the south-east direction is ~600 km. The amplitude loss of the 0.2 Hz signal at a distance of 600 km is 60 dB relative to the amplitude at 1 km from the source.

The observations and the model outputs during the November 2020 event can be summarized as follows: infrasound arrives from sources in the North Atlantic to Central Europe mainly through the stratospheric waveguide formed between the ground and upper stratosphere. The jet-stream disturbance above the eastern North Atlantic does not have an impact on infrasound arrivals in Central Europe on 6th November 2020 at 00 UTC. Fluctuating signal amplitudes are likely a consequence of fluctuating intensity of the microbarom source during maritime storms. The decrease of signal frequency at WBCI is not caused by a transient change in signal ducting and by the related signal filtering in the thermospheric waveguide.

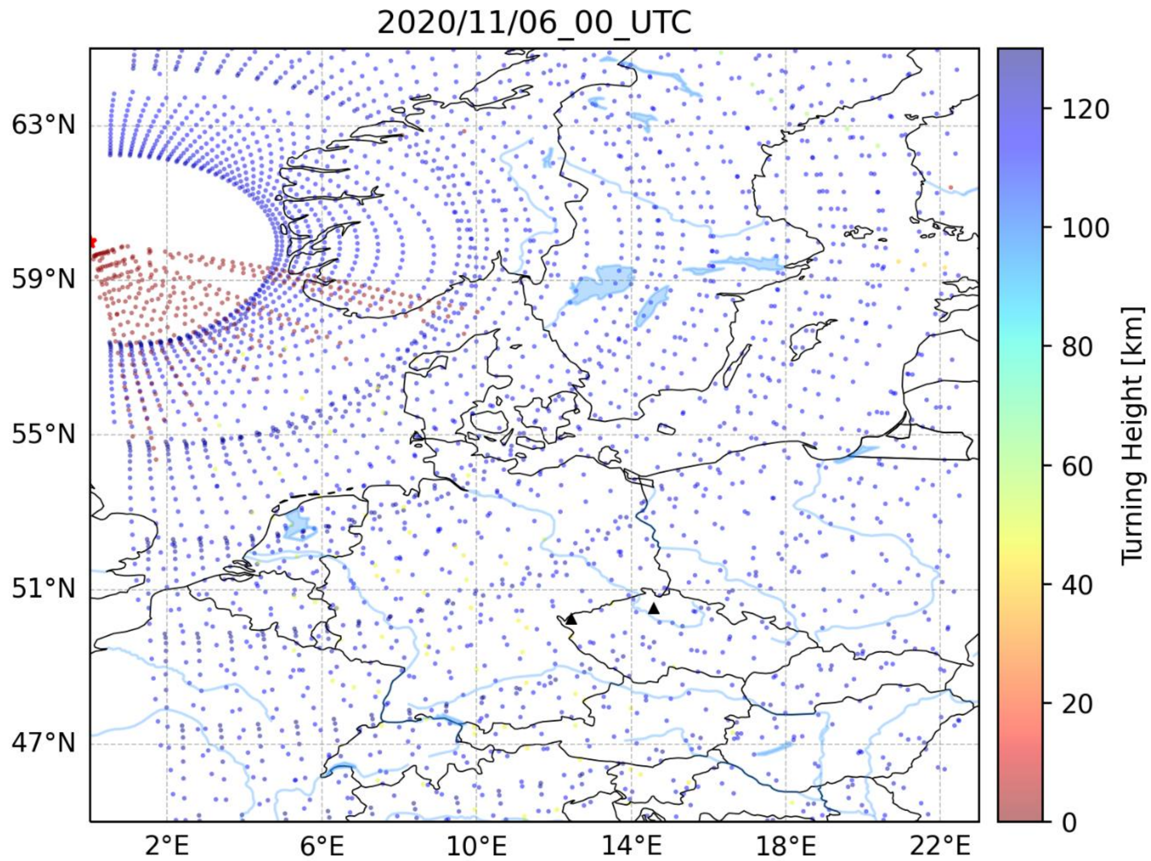

Fig.6. Modelled infrasound propagation from a point source located at 60°N and 0°longitude (red asterisk) during the streamer event on 6th November 2020 at 00 UTC. Colobar refers to the turning height (maximum height) of the signal. Red indicates signal propagation in the

waveguide formed near the tropopause (altitudes around 10 km), arrivals through the thermospheric waveguide are in blue (altitudes above 100 km). Black triangles represent infrasound arrays WBCI (the left triangle) and PVCI (the right triangle).

3.1.2 Infrasound observations from 28th February to 24th March 2021

A streamer event occurred from 9th to 12th March 2021 preceded and followed by calm periods from 28th February to 7th March and from 13th to 24th March, respectively.

The most important phenomenon identified in the infrasound arrival parameters is a fluctuating trace velocity.

Both WBCI and PVCI detect signals arriving from the north-west, from back-azimuths of 285° – 310°. An increase of signal trace velocities is observed in some of the detections at WBCI during the streamer event compared to calm periods (Figure 7). On 10th March at 00 – 06 UTC, trace velocities of 0.460 km/s and 0.380 km/s are observed from back-azimuths of 270° and 310° respectively. It is by 0.05 – 0.13 km/s higher than on the calm days. On the other hand, signals from the back-azimuth of 288° arrive with the trace velocity of 0.330 km/s within the same time window, the velocity corresponds to that on the calm days. Effects of spatial aliasing shall be taken into account when evaluating the detections. The signal frequencies are around 0.2 Hz, well above the range of array optimum performance. The observed different trace velocities at WBCI can therefore be a processing bias rather than a consequence of variations in signal ducting.

In contrast to the WBCI observations, PVCI records a decrease in trace velocities on 10th March at 00 – 06 UTC (Figure 8). Trace velocities of 0.377 km/s are observed compared to 0.413 km/s and 0.395 km/s during the calm periods before and after the streamer, respectively.

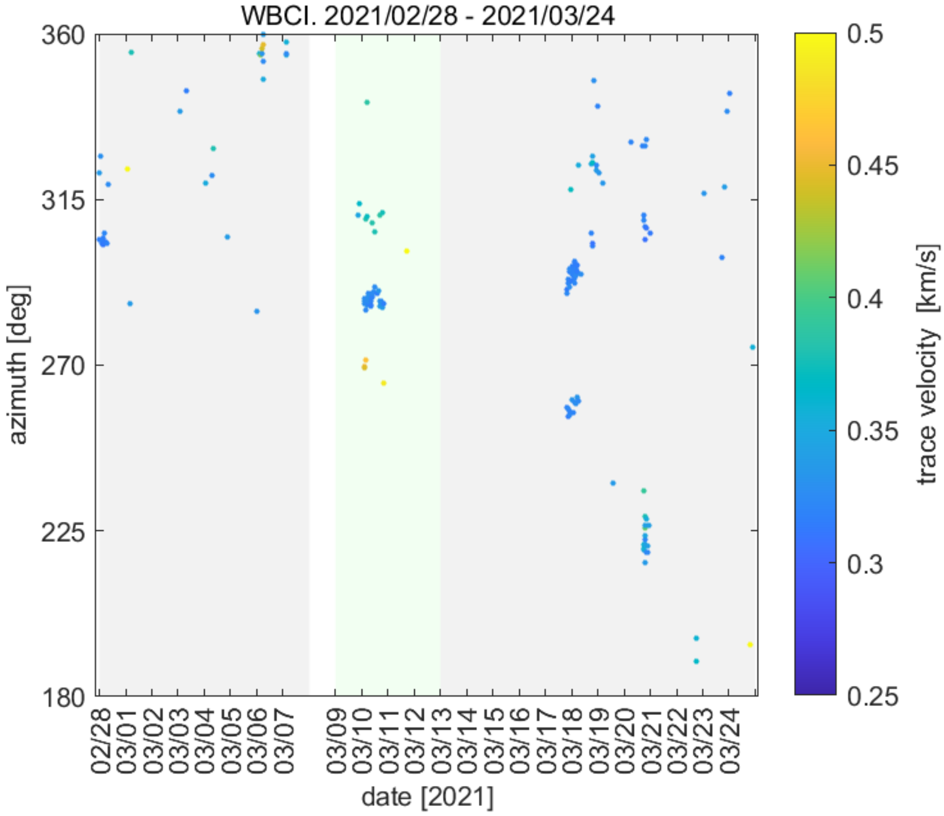

Fig.7. Infrasound observations at WBCI on 28th February – 24th March 2021. Azimuth of signal arrival is shown; the colorbar refers to the signal trace velocity. Green background marks the streamer event, grey background marks the calm periods.

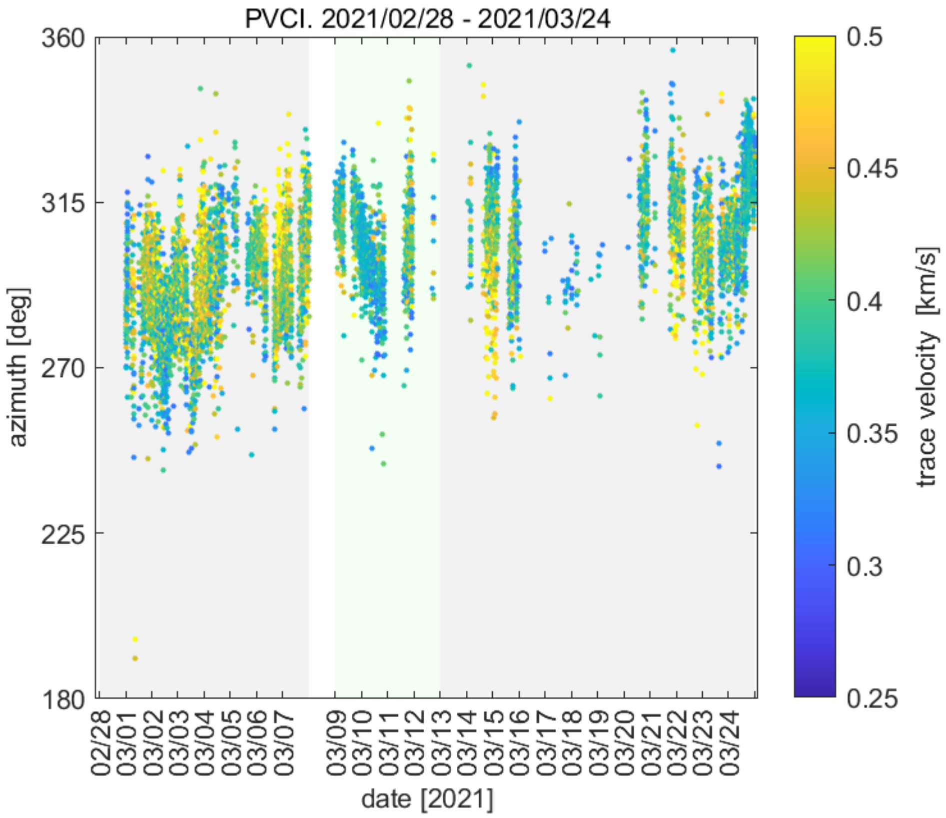

Fig.8. Infrasound observations at PVCI on 28th February – 24th March 2021. Azimuth of signal arrival is shown; the colorbar refers to the signal trace velocity. Green background marks the streamer event, grey background marks the calm periods.

Changes of the trace velocity can indicate changes of the refraction altitude of the signal (Lonzaga, 2015). The exact limits of the trace velocity for the given atmospheric waveguide depend on the current state of the atmosphere. We use the thresholds determined for a model atmosphere in Lonzaga (2015) as helpful hints for our further consideration: Trace velocities below 0.340 km/s indicate signal refraction in the troposphere and lower stratosphere. Trace velocities between 0.340 and 0.380 km/s are typical for signals ducted in the waveguide between the ground and the upper stratosphere. Signals traveling in the thermospheric waveguide arrive with trace velocities larger than 0.380 km/s.

The high trace velocities recorded at PVCI disprove signal refraction in the lower stratosphere. Hence, it is unlikely that the signals arrive through a waveguide that can form at the tropopause – lower stratosphere by the effect of the streamer event.

Like in the November 2020 case, signal propagation above the eastern North Atlantic and Western and Central Europe is investigated using the InfraGA/GeoAc tools. Propagation of the 0.2 Hz signal is modelled on 10th March at 03 UTC. A source is located at 55°N 15°W at a distance of ~2000 km from the stations. This scenario represents signal propagation from the central North Atlantic. The other source is located at 55°N 0°latitude representing propagation of microbaroms from the North Sea. The distance from the stations is ~1000 km.

Eastward signal ducting is enabled in the stratospheric and thermospheric waveguides from both sources to the stations. Strong signal absorption in the thermospheric waveguide likely disables thermospheric arrivals to the PVCI and WBCI. We assume that signals ducted in the upper stratosphere are detected. The other eastward waveguide occurs near the tropopause, formed by the eastward to south-eastward jet-stream above the eastern North Atlantic and Western Europe at latitudes 50 – 60°N Figure 9. Signals from the source in the North Atlantic are predicted to travel in the tropopause waveguide to distances of 1000-1100 km. The signal attenuation is low in the tropopause waveguide; the relatively short distance under the waveguide influence is determined by the location and extent of the jet-stream disturbance. The tropopause/lower stratosphere arrivals can be detected mainly on the British Isles. The waveguide does not reach to PVCI and WBCI stations (see supplementary materials).

Signals emitted by a source in the North Sea can propagate through the tropopause waveguide. The signals propagate to the south-east and are predicted to reach Central Europe. The tropopause/lower stratosphere arrivals are represented by red dots in Figure 10. The influenced regions are to the south-west from PVCI and WBCI, several hundreds of kilometres distant from the stations. The approximation of infrasound propagation obtained from the raytracing is in accord with observations. The trace velocities at PVCI of 0.377 km/s indicate infrasound propagation in the waveguide formed between the ground and the upper stratosphere rather than in the waveguide near the tropopause.

Like in the November 2020 case, infrasound arrivals from the North Atlantic to the stations PVCI and WBCI in Central Europe are not influenced by the waveguide at the tropopause – lower stratosphere. Observed trace velocities fluctuate within or close above the limits that indicate infrasound propagation in the upper stratosphere during the streamer event and both adjacent quiet periods.

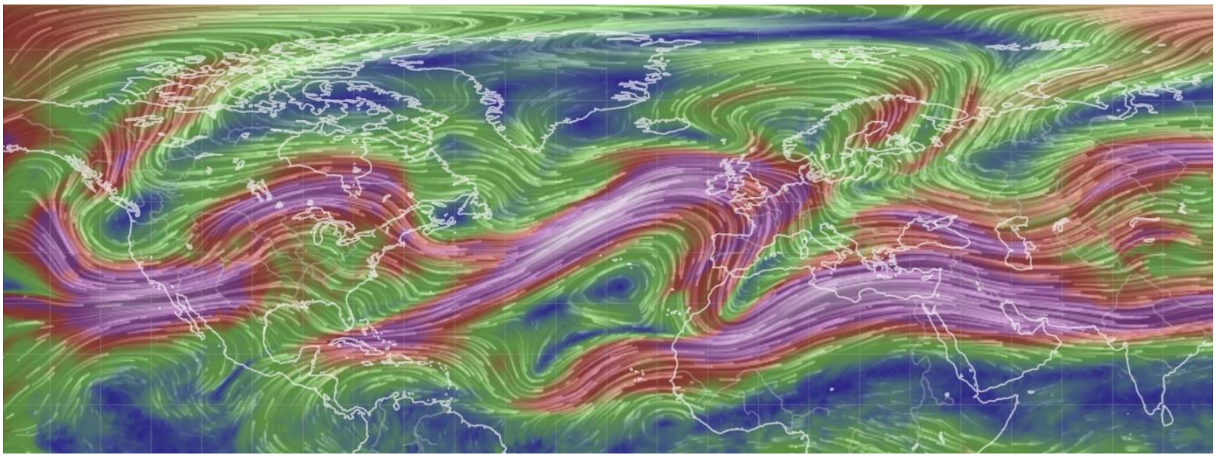

Fig.9. Wind field at the pressure level of *250 hPa* on 10 March 2021 at 03 UTC. A disturbance of the jet-stream above the eastern North Atlantic and the British Isles is caused by the streamer event.

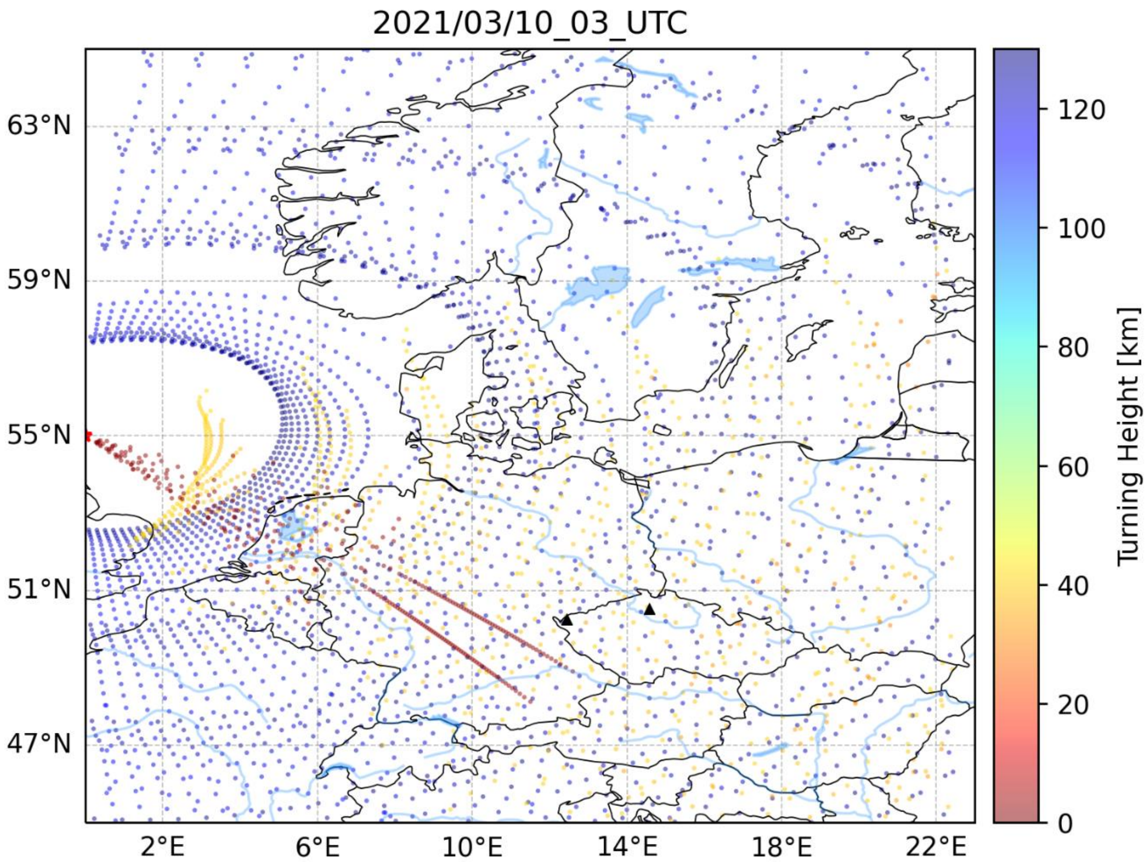

Fig.10 Modelled infrasound propagation from a point source located at 55°N and 0°longitude (red asterisk) on 10th March 2021 at 03 UTC. Colobar refers to the turning height (maximum height) of the signal. Red indicates signal propagation in the waveguide formed near the tropopause (altitudes around 10 km), arrivals through the stratospheric waveguide are in

yellow (altitudes around 40-50 km) and arrivals through the thermospheric waveguide are in blue (altitudes above 100 km). Black triangles represent infrasound arrays WBCI (the left triangle) and PVCI (the right triangle).

3.2 Results and discussion of gravity waves in the troposphere and ionosphere

3.2.1 Investigation of GWs measured on the ground by WBCI array of micro-barometers.

Figure 11 shows the RMS amplitudes of pressure fluctuations in the period range 5-60 min recorded from November 1 to November 9, 2020. This interval covers a distinct streamer event that occurred from November 3 to November 7. The results of propagation analysis are shown in Figure 12, which displays the phase velocities and azimuths of GWs. Only results that satisfied the criterion (dv/v <0.5) and (dAZ<10°) and (p_{RMS}>0.02 Pa) are presented, where dv/v, dAZ, p_{RMS} are the relative uncertainty of GW phase velocity, uncertainty of azimuth and root mean square value of pressure fluctuations in the analysed time interval. Figure 12 demonstrates that there is a tendency for higher phase velocities and occurrence of different azimuths during the streamer event. Therefore, it is useful to compare the GW characteristics during streamer events and calm conditions.

Figure 13 shows histograms obtained by a statistical analysis. The RMS amplitudes of pressure fluctuations in the period range 5 – 60 min, phase velocities and azimuths were investigated separately for calm conditions (upper plots) and for streamer events listed in Table 1 (bottom plots) with a 1-hour time resolution. The solid vertical lines mark lower (Q1) and upper (Q3) quartiles. The dashed vertical lines depict boundaries for large (Q3+1.5·(Q3-Q1)) and extreme (Q3+3·(Q3-Q1)) values. A difference between histograms for RMS pressure fluctuations and azimuths obtained for calm and disturbed conditions is obvious. During the streamer events the azimuths are distributed more randomly and more extreme pressure amplitudes can be observed. A minor difference is also observed for phase velocities.

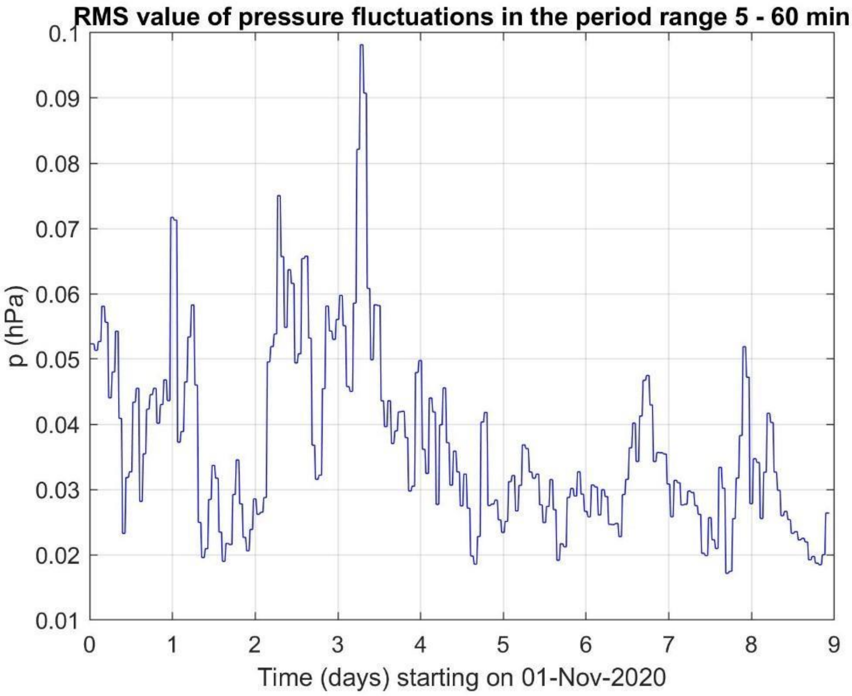

Figure 11 Amplitude of GWs recorded by WBCI from 2020-11-01 to 2020-11-09

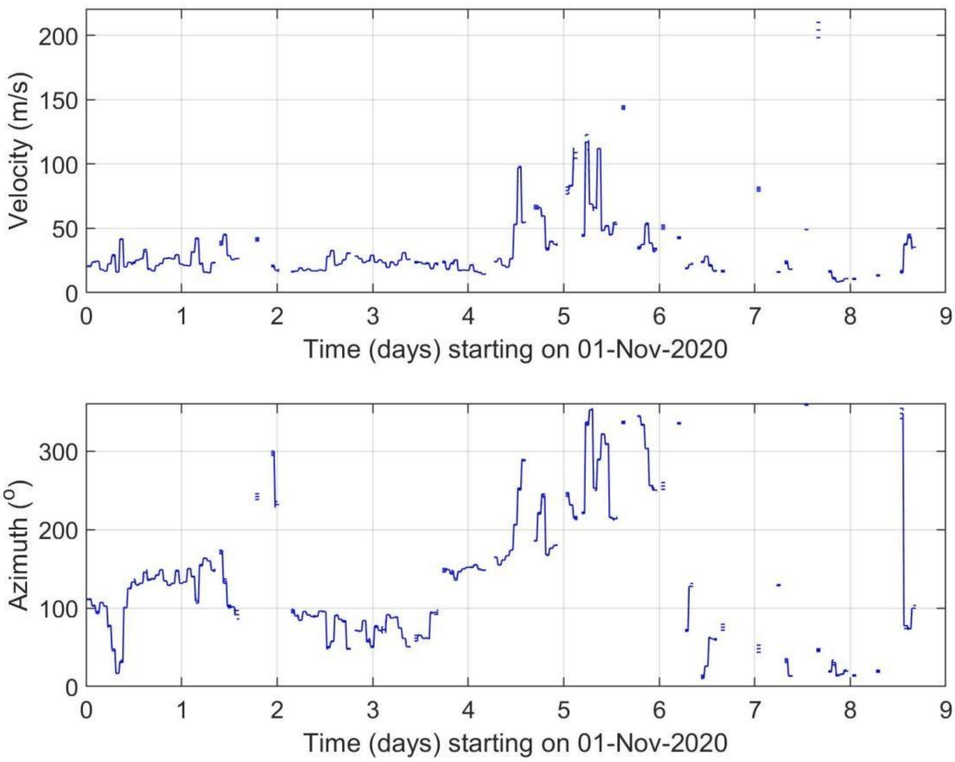

Figure 12 Propagation velocity and azimuth of GWs recorded by WBCI from 2020-11-01 to 2020-11-09

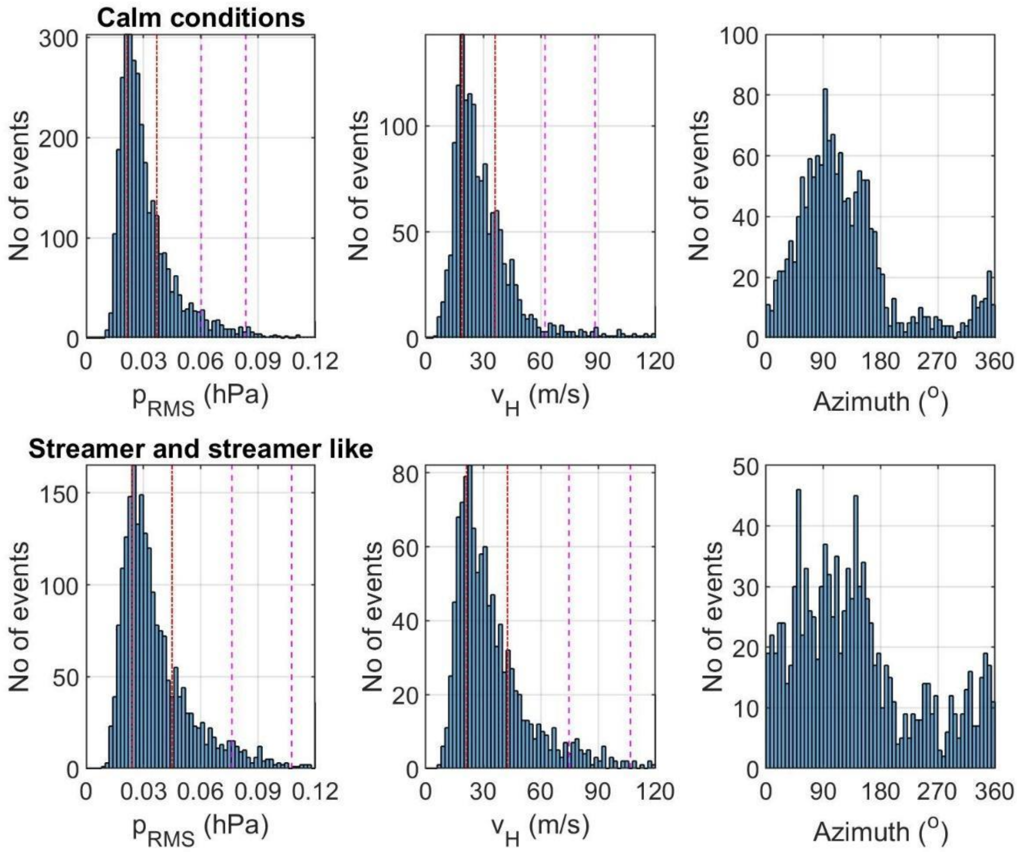

Figure 13 GW characteristics (RMS of pressure fluctuations, phase velocity and azimuth) for calm periods (upper plots) and streamer and streamer like events (bottom plots) for 2020 and winter 2021. The red vertical lines mark lower (Q1) and upper (Q3) quartiles. The dashed magenta vertical lines depict boundaries for large (Q3+1.5·(Q3-Q1)) and extreme (Q3+3·(Q3-Q1)) values.

3.2.2 Investigation of GWs measured in the ionosphere by continuous Doppler sounding system (CDS)

The 2D propagation analysis of GWs was performed using the 2D versions of methods mentioned in Section 2 and in detail described by Chum and Podolská (2018). As discussed in Section 2 and by (Chum et al., 2021), the 2D propagation analysis makes it possible to analyze much larger number of time intervals than the 3D analysis. The propagation analysis obtained for the interval from 1st November to 9th November 2020, which covers the significant streamer event that occurred from 3rd November 2020 to 7th November 2020, is presented in Figure 14. Only results that satisfied the criteria (dv/v <0.2) and (dAZ<20°) and

(f_{DRMS}>0.05 Hz) and (C_{max}<0.5) are presented, where dv/v is the relative uncertainty of GW phase velocity, dAZ is the azimuth uncertainty, f_{DRMS} is the root mean square of the Doppler shift in the analysed time interval and C_{max} is the maximum in the normalized energy map for the best beam (slowness) search; C_{max} is 1 for identical signals (Chum and Podolská, 2018). It is considered that signals are not sufficiently correlated (coherent) for reliable propagation analysis if C_{max} < 0.5 (Chum et al., 2021). The velocities and azimuth obtained by observation at 3.59 MHz are in red, whereas the values based on measurements at 4.65 MHz are in blue. Obviously, the observations at 3.59 MHz mostly correspond to the nighttime, whereas observations at 4.65 MHz were mostly made during the daytime. The 4.65 MHz signal did not reflect from the ionosphere (escaped to the outer space) at night due to the low critical frequency of the ionosphere. On the other hand, the 3.59 MHz signal mostly reflected during the day from the ionospheric E layer and the Doppler shift was negligible, difficult to analyse.The GWs usually propagated roughly poleward at night and roughly equatorward during the daytime. This is fully consistent with the statistical investigation (Chum et al., 2021) which showed that propagation directions of GWs in the ionosphere exhibit diurnal and seasonal behaviour and are mainly controlled by the neutral winds in the thermosphere.

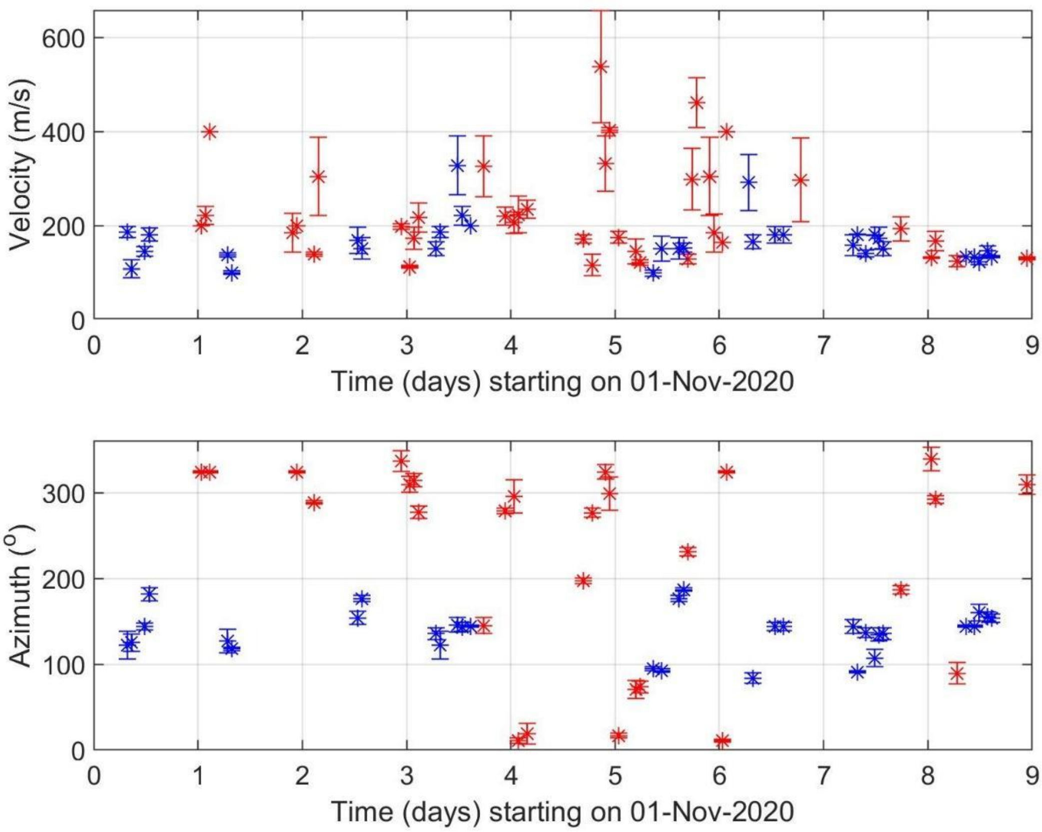

Figure 14 Propagation velocity and azimuth of GWs in the ionosphere obtained using CDS measurements from 2020-11-01 to 2020-11-09. The velocities and azimuth obtained by observation at 3.59 MHz are by red, whereas the values based on measurements at 4.65 MHz are by blue.

Based on the analysis of the GW observed in the ionosphere during the streamer event and on the previous statistical analysis, we conclude that no obvious signature related to streamer event was observed for the propagation of GW the ionosphere.

It should be also mentioned that the phase velocities of GW measured on the ground (Figure 8) and at heights around 200 km in the ionosphere differ. There are several reasons for that. First, the observed horizontal phase velocities depend on the elevation angle of GW propagation and on the ambient temperature as follows from the dispersion relation (the temperature enters the dispersion relation via the buoyancy frequency and the scale height). The temperature in the ionosphere/thermosphere is several times higher than in the troposphere. The elevation angles might change during the upward propagation of GWs, depending on the wind and temperature profile. Second, GWs propagate with a tilt, not vertically upward. It is therefore highly probable that the sources of the GWs observed in the troposphere and ionosphere are different. Moreover, GW can break during their propagation upward and secondary gravity waves might be observed in the ionosphere.

4) Conclusion and discussion

The focus of this study was to test independent types of observations like Doppler sounding and microbarograph measurements for an analysis of GW behavior during streamer events, which are strongly connected with PW or GW and the large scale mass transport of ozone and that is why it can be very interesting for studies of atmospheric dynamics.

We also investigate effects of the streamer events on infrasound propagation. Streamer events are significant disturbances to circulation in the tropopause/lower stratosphere region. Modifications of infrasound ducting in the atmosphere can therefore be expected. Indeed, the InfraGA/GeoAc raytracing tools predict that a waveguide develops at the tropopause during the analyzed streamer events in November 2020 and in March 2021 the direction of which is determined by the disturbed jet-stream and varies from event to event. The tropopause waveguide ducts infrasound up to distances of several hundreds to a thousand of km from the source in a limited azimuth range. The azimuth sector of the extent of 50 – 60° is influenced in the analysed cases. In accord with the model predictions, streamer event related phenomena were not found in infrasound detection at the infrasound stations PVCI and WBCI in Central Europe during the studied cases. The observability of streamer event signatures in infrasound arrival parameters therefore strongly depends on the mutual position of the source, the streamer event disturbance of the tropopause jet-stream and the infrasound station. It can be recommended for future studies to use a dense network of infrasound arrays that covers various directions and distances from the streamer event. Due to the typical occurrence of the streamer events over the North Atlantic, infrasound stations in Western Europe can be of particular interest.

Supplementary ground-based measurements of GW using the WBCI array in the troposphere showed that GW propagation azimuths were more random during streamer and streamer-like events compared to those observed during calm conditions as can be seen from the plots in Figure 13. On the other hand, the GW propagation characteristics observed in the ionosphere by CDS during streamer events did not differ from those expected for the given time period, based on previous statistical studies (Chum et al., 2021).

The results therefore indicate that streamers in the stratosphere might lead to changes in wave propagation in the troposphere. The impact on the ionosphere was not confirmed, but cannot be excluded due to spare and localized observations of GW activity. In general, to validate the preliminary results obtained in this study, a denser measurement network and more streamer events need to be analyzed.

Data availability:

ozone column measurements (TO3) which are available as a service by DLR at https://atmos.eoc.dlr.de/

Ground to space model vertical atmospheric profiles were obtained at https://g2s.ncpa.olemiss.edu/; accessed on 27 January – 4 February 2024

The WAVEWATCHIII® wave-action model data were accessed via ftp at polar.ncep.noaa.gov/waves/JCOMM/2020 on 13-14 March 2023.

The Deutscher Wetterdienst synoptic charts were accessed at https://www2.wetter3.de/archiv_dwd_dt.html on 3 February 2024.

Author contributions

MK and LK create the idea of manuscript; JCh, MK, TS, LK, and KP suggest the datasets and methods; TS, JCh, LK, KP and FT analyzed the data; MK wrote the manuscript draft; JCh, TS, LK and KP reviewed and edited the manuscript.

Competing interests

The authors declare that they have no conflict of interest.

Acknowledgement

The DTK-GPMCC software was kindly provided by Commissariat à l'énergie atomique et aux énergies alternatives, Centre DAM-Île-de-France, Département Analyse, Surveillance, Environnement, Bruyères-le-Châtel, F91297 Arpajon, France.

The authors are grateful to Dr. Phil Blom and Los Alamos National Laboratory for opening the InfraGA/GeoAc tools to the public.

Financial support: This study is supported by LISA project- Lidar measurements to Identify Streamers and analyze Atmospheric waves, AEOLUS-INNOVATION, Contract No. 4000133567/20/I-BG

References

Assink, J.D., Waxler, R., Smets, P., Evers, L.G. (2014). Bidirectional infrasonic ducts associated with sudden stratospheric warm-ing events. J. Geophys. Res. Atmos. 119,1140-1153.

Bittner, M., Höppner, K., Pilger, C., Schmidt, C. (2010). Mesopause temperature perturbations caused bzy infrasonic waves as a potential indicator for the detection of tsunamis and other geo-hazards. Nat. Hazards Earth Syst. Sci., 10, 1431-1442. www.nat-hazards-earth-syst-sci.net/10/1431/2010/doi:10.5194/nhess-10-1431-2010

Blanc, E. (1985). Observations in the upper atmosphere of infrasonic waves from natural or artificial sources: A summary. Ann. Geophys., 3, 673-688.

Blixt, E.M., Nasholm, S.P., Gibbons, S.J., Evers, L.G., Charlton-Perez, A.J., Orsolini, Y.J., Kvaerna, T. (2019). Estimating tropo-spheric and stratospheric winds using infrasound from explosions. J. Acoust. Soc. Am. 146:2.

Blom, P., Waxler, R. (2012). "Impulse propagation in the nocturnal boundary layer: Analysis of the geometric component". *J. Acoust. Soc. Am.,* **131**, 3680 – 3690. doi: 10.1121/1.3699174.

Blom, P. (2019). "Modeling infrasonic propagation through a spherical atmospheric layer: Analysis of the stratospheric pair." *J. Acoust. Soc. Am.,* **145**, 2198–2208. doi: 10.1121/1.5096855.

Bondár I., T. Šindelářová, D. Ghica, U. Mitterbauer, A.Liashchuk, J. Baše, J. Chum, C. Czanik, C. Ionescu, C. Neagoe, M. Pásztor, A. Le Pichon (2022), Central and Eastern European Infrasound Network: Contribution to Infrasound Monitoring, *Geophys. J. Int.*, ggac066, https://doi.org/10.1093/gji/ggac066

Brachet, N., Brown, D., Le Bras R., Cansi, Y., Mialle, P., Coyne, J. (2010). Monitoring the Earth's Atmosphere with the Global IMS Infrasound Network. In: Le Pichon, A., Blanc, E., Hauchecorne A. (Eds.), Infrasound Monitoring for Atmospheric Studies. Springer Science+Business Media B.V., 77-118. Doi: 10.1007/978-1-4020-9508-5_3

Campus, P., Christie, D.R. (2010). Worldwide Observations of Infrasonic Waves. In: Le Pichon, A., Blanc, E., Hauchecorne A. (Eds.), Infrasound Monitoring for Atmospheric Studies. Springer Science+Business Media B.V., 185234-118. Doi: 10.1007/978-1-4020-9508-5_6

Cansi, Y., 1995. An automatic seismic event processing for detection and location: The P.M.C.C. method. Geophys. Res. Lett. 22, 1021-1024. doi: 10.1029/95GL00468

Ceranna, L., Matoza, R., Hupe, P., Le Pichon, A., Landès, M., (2019). Systematic Array Processing of a Decade of Global IMS Infrasound Data. In: Le Pichon, A., Blanc, E., Hauchecorne, A. (eds) Infrasound Monitoring for Atmospheric Studies. Chal-lenges in Middle Atmospheric Dynamics and Societal Benefits. Springer Nature Switzerland AG.

Chum J, Podolská K (2018) 3D analysis of GW propagation in the ionosphere. Geophysical Research Letters, 45, 11,562–11,571, https://doi.org/10.1029/2018GL07969

Chum, J., Podolská, K., Rusz, J., Baše, J., Tedoradze, N. (2021), Statistical investigation of gravity wave characteristics in the ionosphere. Earth Planets Space 73, 60, https://doi.org/10.1186/s40623-021-01379-3

Czech microbarograph network, https://doi.org/10.7914/SN/C9

Drob, D. P., Picone, J. M., Garcés, M. (2003). Global morphology of infrasound propagation. *J. Geophys. Res. Atmospheres*, **108** (D21). doi: 10.1029/2002JD003307.

Evers, L. G., Siegmund, P. (2009). Infrasonic signature of the 2009 major sudden stratosphericwarming, Geophys. Res. Lett., 36, L23808, doi:10.1029/2009GL041323

Evers, L.G., Haak, H.W. (2010). The Characteristics of Infrasound, its Propagation and Some Early History. In: Le Pichon, A., Blanc, E., Hauchecorne, A. (eds) Infrasound Monitoring for Atmospheric Studies. Springer, Dordrecht.

Evers, L. G., van Geyt, A. R. J. , Smets, P., Fricke, J.T. (2012). Anomalous infrasound propagation in a hot stratosphere and the existence of extremely small shadow zones, J. Geophys. Res., 117, D06120, doi:10.1029/2011JD017014.

Eyring, V., Dameris, M., Grewe, V., Langbein, I., & Kouker, W. (2002). Climatologies of streamer events derived from a transport model and a coupled chemistry-climate model.

Fritts, D.C. & Alexander, M.J., (2003). Gravity wave dynamics and effects in the middle atmosphere. Rev. Geophys., 41 (1), 1003.

Garcès, M., Willis, M., Hetzer, C., Le Pichon , A., Drob, D., (2004). On using ocean swells for continuous infrasonic measurements of winds and temperature in the lower, middle, and upper atmosphere. Geophys. Res. Lett. 31, L19304. doi: 10.1029/2004GL020696

Garcès, M.A., (2013). On infrasound standards, part 1: Time, frequency, and energy scaling. InfraMatics 2, 13-35. doi: 10.4236/inframatics.2013.22002

Georges, T.M. (1968). H. F. Doppler studies of travelling ionospheric disturbances. J. Atmos.Terr. Phys., 30, 735-746.

Gerlach, C., Földvary, L., Švehla, D., Gruber, T., Wermuth, M., Sneeuw, N., ... & Steigenberger, P. (2003). A CHAMP-only gravity field model from kinematic orbits using the energy integral. Geophysical Research Letters, 30(20).

Hersbach, H., Bell, B., Berrisford, P., Hirahara, S., Horányi, A., Muñoz-Sabater, J., ... & Thépaut, J. N. (2020). The ERA5 global reanalysis. Quarterly Journal of the Royal Meteorological Society, 146(730), 1999-2049.

Hupe, P., Ceranna, L., Pilger, C., de Carlo, M., Le Pichon, A., Kaifler, B., Rapp, M. (2019). Assessing middle atmosphere weather models using infrasound detections from microbaroms. Geophys. J. Int., 216, 1761–1767 doi: 10.1093/gji/ggy520

James, P. M. (1998): A climatology of ozone mini-holes over the Northern Hemisphere. International Journal of Climatology: A Journal of the Royal Meteorological Society, 18, 12: 12871303

Kramer, R, S. Wüst, and M. Bittner (2016). Investigation of gravity wave activity based on operational radiosonde data from 13 years (1997-2009): Climatology and possible induced variability, Journal of Atmospheric and Solar-Terrestrial Physics 140, 23–33; http://dx.doi.org/10.1016/j.jastp.2016.01.014

Kramer, R., S. Wüst, C. Schmidt, and M. Bittner (2015). Gravity wave characteristics in the middle atmosphere during the CESAR campaign at Palma de Mallorca in 2011/2012: Impact of extratropical cyclones and cold fronts, Journal of Atmospheric and Solar-Terrestrial Physics 128 (2015) 8–23, http://dx.doi.org/10.1016/j.jastp.2015.03.001

Kai Ming Huang, Shao Dong Zhang, Fan Yi, (2010).Reflection and transmission of atmospheric gravity waves in a stably sheared horizontal wind field, Journal of Geophysical Research: Atmospheres, 10.1029/2009JD012687, **115**, D16,

Landès, M., Ceranna, L., Le Pichon, A., & Matoza, R. S. (2012). Localization of microbarom sources using the IMS infrasound network. Journal of Geophysical Research: Atmospheres, 117(D6).

Le Pichon, A., Cansi, Y. (2003). PMCC for infrasound data processing. InfraMatics 02, 1-9.

Le Pichon, A., Blanc, E., (2005). Probing high-altitude winds using infrasound. J. Geophys. Res., 110, D20104. doi: 10.1029/2005JD006020

Le Pichon, A., Ceranna, L., Garcès, M., Drob, D., Millet, C., (2006). On using infrasound from interacting ocean swells for global continuous measurements of winds and temperature in the stratosphere. J. Geophys. Res., 111, D11106. doi: 10.1029/2005JD006690

Le Pichon, A., Vergoz, J., Blanc, E., Guilbert, J., Ceranna, L., Evers, L., Brachet, N., (2009). Assessing the performance of the International Monitoring System's infrasound network: Geographical coverage and temporal variabilities. J. Geophys. Res. 114, D08112. doi: 10.1029/2008JD010907

Leovy, C. B., Sun, C. R., Hitchman, M. H., Remsberg, E. E., Russell III, J. M., Gordley, L. L., ... & Lyjak, L. V. (1985). Transport of ozone in the middle stratosphere: Evidence for planetary wave breaking. Journal of Atmospheric Sciences, 42(3), 230-244.

Lonzaga, J.B., (2015). A theoretical relation between the celerity and trace velocity of infrasonic phases, J. Acoust. Soc. Am., 138, EL242-EL247. http://dx.doi.org/10.1121/1.4929628

Loyola D.G., Koukouli M.E., Valks P., Balis D.S., Hao N., van Roozendael M., Spurr R.J.D., Zimmer W., Kiemle S., Lerot C., Lambert J.-C. (2011) The GOME-2 total column ozone product: Retrieval algorithm and ground-based validation, Journal of Geophysical Research, vol. 116, D07302, Wiley-Blackwell

Marty, J., (2019). The IMS Infrasound Network: Current Status and Technolofical Developments, in: Le Pichon, A., Blanc, E., Hauchecorn, A. (Eds.), Infrasound Monitoring for Atmospheric Studies. Challenges in Middle Atmosphere Dynamics and Societal Benefits. Springer Nature Switzerland AG, pp. 3–62. doi:10.1007/978-3-319-75140-5_1

McIntyre, M. E., & Palmer, T. N. (1983). Breaking planetary waves in the stratosphere. Nature, 305(5935), 593-600.

Munro, R., Eisinger, M., Anderson, C., Callies, J., Corpaccioli, E., Lang, R., ... & Albinana, A. P. (2006, June). GOME-2 on MetOp. In Proc. of The 2006 EUMETSAT Meteorological Satellite Conference, Helsinki, Finland (Vol. 1216, p. 48).

Munro, R., et al. (2016): The GOME-2 instrument on the Metop series of satellites: instrument design, calibration, and level 1 data processing – an overview, Atmos. Meas. Tech., 9, 1279–1301, https://doi.org/10.5194/amt-9-1279-2016.

Peters, D., Hoffmann, P., & Alpers, M. (2003). On the appearance of inertia-gravity waves on the north-easterly side of an anticyclone. Meteorologische Zeitschrift, 12(1), 25-35

Polvani, L. M., & Plumb, R. A. (1992). Rossby wave breaking, microbreaking, filamentation, and secondary vortex formation: The dynamics of a perturbed vortex. Journal of Atmospheric Sciences, 49(6), 462-476.

Pramitha, M., Venkat Ratnam, M., Taori, A., Krishna Murthy, B. V., Pallamraju, D., and Vijaya Bhaskar Rao, S. (2015). Evidence for tropospheric wind shear excitation of high-phase-speed gravity waves reaching the mesosphere using the ray-tracing technique, Atmos. Chem. Phys., 15, 2709–2721, https://doi.org/10.5194/acp-15-2709-2015.

Rauthe, M., Gerding, M., Höffner, J., & Lübken, F. J. (2006). Lidar temperature measurements of gravity waves over Kühlungsborn (54° N) from 1 to 105 km: A winter-summer comparison. Journal of Geophysical Research: Atmospheres, 111(D24).

Wüst, S., & Bittner, M. (2006). Non-linear resonant wave–wave interaction (triad): Case studies based on rocket data and first application to satellite data. Journal of atmospheric and solar-terrestrial physics, 68(9), 959-976.

Wüst, S., Offenwanger, T., Schmidt, C., Bittner, M., Jacobi, C., Stober, G., Yee, J.H., Mlynczak, M. G. & Russell III, J. M. (2018). Derivation of gravity wave intrinsic parameters and vertical wavelength using a single scanning OH (3-1) airglow spectrometer. Atmospheric Measurement Techniques, 11(5), 2937-2947.

Smets, P.S.M., Evers, L.G. (2014). The life cycle of a sudden stratospheric warming from infrasonic ambient noise observa-tions, J. Geophys. Res. Atmos., 119, 12,084-12,099

Spurr, R., Loyola, D., Heue, K. P., Van Roozendael, M., & Lerot, C. (2022). S5P/TROPOMI Total Ozone ATBD. Deutsches Zentrum für Luft- und Raumfahrt (German Aerospace Center), Weßling, Germany, Tech. Rep. S5P-L2-DLR-ATBD-400A.

Sutherland, L.C., Bass, H.E., (2004). Atmospheric absorption in the atmosphere up to 160 km. *J. Acoust. Soc. Am.*, 115, 1012–1032. https://doi.org/10.1121/1.1631937

Szuberla, C.A.L., Olson, J.V., (2004). Uncertainties associated with parameter estimation in atmospheric infrasound rays. J. Acoust. Soc. Am. 115, 253-258. doi: 10.1121/1.1635407

Veefkind, J. P., Aben, I., McMullan, K., Förster, H., De Vries, J., Otter, G., ... & Levelt, P. F. (2012). TROPOMI on the ESA Sentinel-5 Precursor: A GMES mission for global observations of the atmospheric composition for climate, air quality and ozone layer applications. Remote sensing of environment, 120, 70-83.